Research Square

Preprints are preliminary reports that have not undergone peer review.
They should not be considered conclusive, used to inform clinical practice,
or referenced by the media as validated information.

A Geometric Approach to Solving Kinematic Problems via Space-Time Graphical Models

Alexander Bogoroditskiy

a.g.bogoroditskiy@gmail.com

Independent Researcher

Physical Sciences - Article

Keywords:

Posted Date: November 19th, 2026

DOI: https://doi.org/10.21203/rs.3.rs-11762536/v1

License: This work is licensed under a Creative Commons Attribution 4.0 International License.
Read Full License

Additional Declarations: There is **NO** Competing Interest.

A Geometric Approach to Solving Kinematic Problems via Space-Time Graphical Models

Alexander G. Bogoroditskiy

Independent Researcher, Saratov, Russia
ORCID: 0009-0008-4036-1114
E-mail: a.g.bogoroditskiy@gmail.com

The great majority of relativistic problems, ranging from particle physics to cosmology, are successfully solved within Einstein's framework. Meanwhile, accelerating computations by streamlining heavy numerical routines, particularly through graphical techniques, is gaining significant interest. However, graphical methods are traditionally treated as tools for visualizing and illustrating relativistic phenomena rather than for practical or analytical problem solving. Here, using the example of inertial particle objects and observers in a 2D spacetime and relying on the premises of Special Relativity (SR), we show that such kinematic problems can be solved by a purely graphical method including the geometry of Loedel's diagram. Within this approach we develop a Space-Time Graphical Model aimed at representing the coordinates and proper time of a selected object for a considered observer at a single scale. Successively, we construct separate models for stationary and moving observers, complying with the relative velocity, and use these same-scale models to read the desired outcome in numerical or analytical forms. The new calculations-free approach is fully consistent with SR and provides a quick solution for a countable number of objects and observers, advantageously supplementing coordinates with proper time for each represented object. While retaining considerable potential for further development, the described geometric core may already be useful for practical applications.

Introduction

Scientific research has significantly advanced since Einstein introduced the Special Theory of Relativity (SR)[1] and Minkowski proposed his Spacetime Diagram (STD)[2] for its illustration at the beginning of the 20th century. While Einstein's framework provides exact solutions to the vast majority of spacetime problems, some tasks require substantial effort. This prompts to seek alternative approaches simplifying problem solving, e.g., recent graphical methods by Benedetto[3] or Maritz[4]. The latter expanded the symmetry of Loedel's STD, transforming observers' systems via a proposed universal tool that is akin to the subsequent considerations.

The approach herein involves four steps. Step 1 relying on the SR premises[1] and running parallel to Bondi's idea of a radar usage[5] gives a particular graphical interpretation to an event image. In Step 2 this interpretation allows us to construct a Space-Time Graphical Model (STGM) providing coordinates and proper times of countably many objects for the initial observer at a single scale. Therewith we derive a universal pattern including the geometry of Loedel's diagram[6] and apply it in Steps 3 and 4 to construct the model for the second observer, complying with the relative velocity and using the same scale (more truly, the same axis graduation). Finally, the identical axis graduation of both models combined with the developed graphical techniques enable us to read and/or compare all presented spatio-temporal data and thus to solve the kinematic problem without any calculations, obtaining the results as numerical values, equations, or analytical expressions.

Case by case, the constructed models are shown to be fully consistent with Einstein's relativity, including the spacetime interval invariance, the Lorentz transformations and the velocity-addition formula.

The geometrical approach matches in physics to the signal usage proposed by Einstein[1] and Bondi[5] and in geometry to the ideas of axes rotations, suggested by Poincaré,[7] Minkowski[2] and Loedel.[6] The angle between time axes, being obtained when developing the method, is analogous to that of the symmetric STD which was designed by Gruner and Sauter[8] in 1921 and rediscovered by Loedel[6] in 1948. The method is compared to the STD in Discussion.

Preliminaries

In our study we employ four similar agents: two inertial particle objects, IO*n* and IO*k*, and two inertial particle observers (watchers), IW*i* and IW*j*, all placed into a 2D conceptual spacetime (*n*, *k*, *i* and *j* are

different individual numbers). We equip these agents with identical clocks to measure proper time expressed as *ct* (*c* is the light speed), and additionally provide the observers with transmitters and receivers, which can be assembled with their clocks for radar measurements.

Since we intend to talk about various agents, it becomes necessary to set a *general rule for subscripts* for unique identification of designations.

We use a single subscript (*i* or *j*) in designations related to a main observer, for example:

bolded $\boldsymbol{ct_i}$ is the time axis of IW*i*, or the main axis. In this study we consider *all axes* to be simple graduated lines, which are *not forming coordinate plane* (see Discussion for details).

All designations related to objects and to a new (or outside) observer will contain double numerical subscript. The first index is the number of the selected IO and the second is the number of the main IW who is directly relevant (or pertaining) to the designated entities, for example:

r_{ni} is the radar distance to IO*n*, measured by IW*i*;

bolded $\boldsymbol{ct_{ni}}$ and $\boldsymbol{x_{ni}}$ are the time and space axes representing IO*n* for IW*i*.

V_{ni} is the projection of IO*n*'s velocity on space axis $\boldsymbol{x_{ni}}$, or (in short for 2D) it is IO*n*'s velocity, measured by IW*i*.

We use capital letters to denote point events under consideration: collisions and interactions with radar signals (emission, reflection and detection). We should also imprint the event name in the index of all designations, related to the event, e.g.,

ct_{iB} and x_{iB} are time and space coordinates of event B, valid for IW*i*, and

ct_{niB} is the instant of proper time or simply *instant* shown by IO*n*'s clock at participation in event B; represented for IW*i*.

B_{ni} is the graphical image of IO*n* participating in event B, valid for IW*i*.

Blue and red colours of further drawings correspond to the observers' numbers *i* and *j*. We define the single-colour drawing, constructed for concrete IW, as a *Space-time graphical model* (STGM).

STGM method development

It should be noted in the context of further graphical construction, that each of the inertial agents exists on individual time axis. On such an axis, any point represents the agent's instantaneous image and the respective instant shown by his clock. It is important to emphasize, that this applies to any object or observer.

Step 1. Graphical image of event

Let us start drawing a scheme of a simple physical scenario in which observer IW*i* measures a nonzero radar distance, $r_{ni}\neq 0$, to object IO*n* moving at velocity $V_{ni}\neq 0$.

We draw in Fig. 1 main axis $\boldsymbol{ct_i}$ and mark point E to indicate the position of IW*i* when emitting a radar signal towards IO*n* at instant ct_{iE}. After the subsequent reflection denoted as distant event B, the signal comes back to IW*i* at point D (D≠E), at instant ct_{iD}.

One can easily calculate from the time data, measured by IW*i*'s clock, that event B has happened at instant ct_{iA}, when IW*i* was at point A,

$$ct_{iA} = \frac{ct_{iE}+ct_{iD}}{2} = ct_{iE} + \frac{ct_{iD}-ct_{iE}}{2} = ct_{iE} + \frac{|\mathrm{ED}|}{2} = ct_{iE} + |\mathrm{AE}| \qquad (1)$$

and the distance between IO*n* and IW*i*, r_{niB}, at this instant was

$$r_{niB} = \frac{ct_{iD}-ct_{iE}}{2} = \frac{|\mathrm{ED}|}{2} = |\mathrm{AE}| \qquad (2)$$

The considered radar scenario as well as the chains of relations (1) and (2) are surprisingly similar to Einstein's basic premises.[1] We see that every time when we perform radar measurements, we repeat the signal exchange scheme for clocks synchronization. And two clocks are synchronized when they show the values satisfying relation $t_B - t_A = t'_A - t_B$,[1] where t_A and t'_A are the same to t_{iE} and t_{iD}, respectively, and t_B is the time shown by the other 'stationary clock'[1] at the location of event B. Einstein establishes t_B as the time coordinate of the distant event on the condition that said relation is true. But if we rewrite the

latter as $t_B=(t_A+t'_A)/2$, it becomes similar to the first relation in chain (1). Consequently, t_{iA} has the same value as t_B. Hence in our consideration we may use ct_{iA} as the time coordinate of distant event B: $ct_{iA}=ct_{iB}$.

In the same paragraph Einstein gives the ratio for the speed of light:[1] $2AB/(t'_A-t_A)=c$ and assumes its constancy. In our case, distance AB is denoted r_{niB}, and we may immediately derive the first relation in (2), directly applying this postulate.

Thus, we use the proper time data, measured by the single clock of observer IW*i*, and constancy of lightspeed instead of 'additional stationary clock' and 'measuring rod', to define the time and space coordinates of distant event B:

$$ct_{iB} = ct_{iA}\,, \tag{3}$$

$$x_{iB} = \mathrm{sgn}(x_{iB}) \cdot r_{niB}\,, \tag{4}$$

where sign function "sgn" is applied to specify the direction of observation. With (1) and (2) we obtain

$$\begin{cases} ct_{iB} = ct_{iA} = ct_{iE} + \frac{ct_{iD}-ct_{iE}}{2} = ct_{iE} + \frac{|\mathrm{ED}|}{2} = ct_{iE} + |\mathrm{AE}| \\ x_{iB} = \mathrm{sgn}(x_{iB}) \cdot r_{niB} = \mathrm{sgn}(x_{iB})\frac{ct_{iD}-ct_{iE}}{2} = \mathrm{sgn}(x_{iB})\frac{|\mathrm{ED}|}{2} = \mathrm{sgn}(x_{iB})\,|\mathrm{AE}| \end{cases} \tag{5}$$

Now we assert that we do not have any conventional set of axes: the correct orientation of the space axis is truly unknown. Nevertheless, serving as zero line for space coordinates, time axis $\boldsymbol{ct_i}$ bisects the plane in Fig. 1; and as generally accepted, the right half-plane is defined to contain points with positive space coordinates.

System of chains (5) has a simple graphical solution: it is satisfied by any point, plotted in accordance to the sign of x_{iB} and at distance $r_{niB}=|x_{iB}|=½|\mathrm{ED}|=|\mathrm{AE}|$, measured outward from point A, which is the midpoint of line segment [ED] ($|\mathrm{EA}|=|\mathrm{AD}|$). This determines the semicircle with radius $r_{iB}=r_{niB}=|\mathrm{AE}|$ centred at A, and attached to the left (if $x_{iB}<0$) or to the right (if $x_{iB}>0$, as in Fig. 1) side of main axis $\boldsymbol{ct_i}$. Endpoints E and D of the semicircle should be empty, because they mark instants ct_{iE} and ct_{iD} differing from ct_{iA}, and their space coordinate is zero $x_{iE}=x_{iD}=0\neq r_{ni}$.

Thus, it appears that each point of this semicircle suits to the set of coordinates of event B given by (5).

Aiming to use a reasonably clear term, we refer to the *semicircle* as the instantaneous *graphical image of distant event B*, valid for IW*i*. Looking ahead we may clarify that the semicircle contains images of all potential participants of the event. (Some physical interpretation is also proposed in the Discussion.)

Such a semicircle permits two parallel notations, based on endpoints E and D or on centre A and radius r_{iB}:

$$\text{ᘐED}^- \Leftrightarrow O^-(\mathrm{A},\, r_{iB}=|x_{iB}|),\ \text{for } x_{iB}<0 \text{ and similarly } \text{ᘐED}^+ \Leftrightarrow O^+(\mathrm{A},\, r_{iB}=|x_{iB}|),\ \text{for } x_{iB}>0 \tag{6}$$

It is clear, that when the radius of a semicircle decreases to zero, the semicircle degenerates into a point, and this means that a distant event of radar signal reflection turns into a local event of collision between IO*n* and IW*i*.

As one can see, the above-stated coordinates of distant event B ($ct_{iB}=ct_{iA}$, $x_{iB}=|\mathrm{AE}|$) are *referenced* to the *image* of IW*i* at instant ct_{iA}, labeled as A. Moreover, the coordinates of local events E (ct_{iE}, $x_{iE}=0$) and D (ct_{iD}, $x_{iD}=0$) are also consistent with a similar description. Thus, it becomes evident that in our analysis the IW's image functionally serves as the *reference point* for all observed events.

Step 2. Constructing observer-object graphical model

We continue the physical scenario started in Step 1 (see Fig. 1). At a new point L on axis $\boldsymbol{ct_i}$, IW*i* repeats the emission. After the subsequent reflection, denoted as event P, the signal returns to IW*i* at point N.

Following (5) and (6), we represent this distant event P as new semicircle $\text{ᘐLN}^+=O^+(\mathrm{F},\, r_{iP}=|x_{iP}|=|\mathrm{FL}|)$ centred at reference point F, $|\mathrm{FL}|=|\mathrm{FN}|$ (r_{iP} is the semicircle's radius and x_{iP} is the space coordinate of event P; Fig. 1 satisfies $x_{iB}>x_{iP}>0$, $V_{ni}<0$).

According to the initial idea, IO*n* exists on his time axis $\boldsymbol{ct_{ni}}$. And due to IO*n*'s participation in events B and P, $\boldsymbol{ct_{ni}}$ should pass through two points corresponding to the events' coordinates. Hence, we construct $\boldsymbol{ct_{ni}}$ in Fig. 1 as the tangent to both blue semicircles and name the tangent points: B_{ni} and P_{ni}. Now, we

connect A with B_{ni} and F with P_{ni} by movable space axis $\boldsymbol{x_{ni}}$. To clarify, there is no logical inconsistency in these connections: fundamentally any space axis consists of simultaneous points, and the connected points are *simultaneous*, insomuch as each point of the semicircle has the time coordinate of its centre (see (5), (6), Step 1). Furthermore, we may decide to employ a reference point (such as A or F) as the origin of the space axis, and since this point also marks the current position of IW, the space axis becomes *movable*.

Points B_{ni} and P_{ni} belonging to the semicircles mark on the lower and upper instances (replicas) of $\boldsymbol{x_{ni}}$ the following lengths

$$|x_{niB}| = |\mathrm{AB}_{ni}| = r_{iB} = |x_{iB}| \qquad \text{and} \qquad |x_{niP}| = |\mathrm{FP}_{ni}| = r_{iP} = |x_{iP}| \tag{7}$$

We can also observe in Fig. 1 that time axes $\boldsymbol{ct_i}$ and $\boldsymbol{ct_{ni}}$ intersect at collision point M_i and form angle ψ_{ni}

$$\widehat{\overrightarrow{ct_i}\ \overrightarrow{ct_{ni}}} = \psi_{ni} \tag{8}$$

Considering perpendicularity of tangent and radius, we can note that

$$\overrightarrow{x_{ni}} \perp \overrightarrow{ct_{ni}} \tag{9}$$

with (8) it means:

$$\widehat{\overrightarrow{ct_i}\ \overrightarrow{x_{ni}}} = \mathrm{sgn}(x_{iB}) \cdot \frac{\pi}{2} + \psi_{ni}\ . \tag{10}$$

Since, by (9), triangle $\measuredangle \mathrm{FP}_{ni}\mathrm{M}_i$ is right-angled, the sine of tilt angle ψ_{ni} equals to the ratio $|\mathrm{FP}_{ni}|/|\mathrm{FM}_i|$. Proceeding below, we substitute $|\mathrm{FP}_{ni}|=|x_{iP}|$ from (7) and convert time period $|\mathrm{FM}_i|=ct_{iM}-ct_{iF}$. Applying (3) to the reference point F of event P yields $ct_{iF}=ct_{iP}$. Finally, we use the object's velocity V_{ni} to express space coordinate $|x_{iP}|$, thus obtaining

$$|\sin\psi_{ni}| = \frac{|\mathrm{FP}_{ni}|}{|\mathrm{FM}_i|} = \frac{|x_{iP}|}{ct_{iM}-ct_{iF}} = \frac{|x_{iP}|}{ct_{iM}-ct_{iP}} = \frac{(t_{iM}-t_{iP})|V_{ni}|}{(t_{iM}-t_{iP})c} = \frac{|V_{ni}|}{c}$$

When dropping modulus $$\sin\psi_{ni} = \frac{V_{ni}}{c}\,, \tag{11}$$

a rule aligning the signs of ψ_{ni} and V_{ni} is required. We propose to define ψ_{ni} as *positive* ($\psi_{ni}>0$) when it is *clockwise* from main axis $\boldsymbol{ct_i}$ to object's axis $\boldsymbol{ct_{ni}}$ (this resembles azimuth). Angle ψ_{ni} retains its sign in (8), (10), and (11). In Fig. 1, the counterclockwise direction of ψ_{ni} sets $\psi_{ni}<0$ and via (11) yields $V_{ni}<0$.

From (11), the range of ψ_{ni} is: $-\frac{\pi}{2} < \psi_{ni} < \frac{\pi}{2}$, when $-c < V_{ni} < c$.

Substituting $V_{ni}=0$ in (11) yields $\psi_{ni}=0$ meaning $\boldsymbol{x_{ni}} \perp \boldsymbol{ct_i}$ (10) as in the Cartesian system, but lacked coordinate plane. Assuming $V_{ni}=-c$ yields $\psi_{ni}=-\frac{1}{2}\pi$ and turns $\boldsymbol{ct_{ni}} \perp \boldsymbol{ct_i}$ with the left direction of $\boldsymbol{ct_{ni}}$ (8); as the result event points M_i and P_{ni} (labeled in Fig. 1) merge into N implying now the triple local event. Setting $V_{ni}=c$ ($\psi_{ni}=\frac{1}{2}\pi$) reverses $\boldsymbol{ct_{ni}}$ and causes points M_i, P_{ni} and N to merge into L. (In the last two cases the radar distances are zero.) As an illustration, the 'time line' of light ($|V_{ni}|=c$) is always perpendicular to the main time axis in STGM.

The relations (8)–(11) reveal the key geometric features of the STGM axes.

In light of Eq. (5)–(7) and Fig. 1, we applied the identical unit lengths to the axes $\boldsymbol{ct_i}$ and $\boldsymbol{x_{ni}}$. And now we are going to verify the scale of IO*n*'s axis $\boldsymbol{ct_{ni}}$.

Derivation 1. Spacetime interval invariance.

From point P_{ni} in Fig. 1, we draw a green segment parallel to main axis $\boldsymbol{ct_i}$ until it intersects (at G) the lower replica of space axis $\boldsymbol{x_{ni}}$. Thereby, we obtain parallelogram $\square\mathrm{AFP}_{ni}\mathrm{G}$ and right-angled (9) triangle $\measuredangle \mathrm{GB}_{ni}\mathrm{P}_{ni}$.

Let us express each side of $\measuredangle \mathrm{GB}_{ni}\mathrm{P}_{ni}$ as a time or space interval.

In the relation below we replace hypotenuse $|\mathrm{GP}_{ni}|$ with $|\mathrm{AF}|$ as the opposite side of $\square\mathrm{AFP}_{ni}\mathrm{G}$. Then we convert time period $|\mathrm{AF}|=ct_{iF}-ct_{iA}$. Further, since F and A are the reference points of events P and B, we follow (3) to substitute $ct_{iP}=ct_{iF}$ and $ct_{iB}=ct_{iA}$

$$|\mathrm{GP}_{ni}| = |\mathrm{AF}| = |ct_{iF} - ct_{iA}| = |ct_{iP} - ct_{iB}| \tag{12}$$

We move on to leg $|GB_{ni}|$, and decompose it as the part of segment $|AB_{ni}|$; then we replace subtracted $|AG|$ by $|FP_{ni}|$, using parallelogram $\square AFP_{ni}G$ (see Fig. 1), and substitute the space values from (7):

$$|GB_{ni}| = |AB_{ni}| - |AG| = |AB_{ni}| - |FP_{ni}| = |x_{niB} - x_{niP}| = |x_{iB} - x_{iP}| \quad (13)$$

The last side $|B_{ni}P_{ni}|$ lying on the object's time axis $\boldsymbol{ct_{ni}}$ is thought to be the duration between local (for IOn) events B and P, measured by IOn's clock

$$|B_{ni}P_{ni}| = |ct_{niP} - ct_{niB}| \quad (14)$$

and to check this, we apply to $\measuredangle GB_{ni}P_{ni}$ the Pythagoras theorem $|GP_{ni}|^2 = |GB_{ni}|^2 + |B_{ni}P_{ni}|^2$ as

$$|GP_{ni}|^2 - |GB_{ni}|^2 = |B_{ni}P_{ni}|^2 \quad (15)$$

After substituting (12)–(14) in (15), we obtain

$$(ct_{iP} - ct_{iB})^2 - (x_{iB} - x_{iP})^2 = (ct_{niP} - ct_{niB})^2 \quad (16)$$

On the left and on the right of (16), we see squares of the spacetime intervals between events P and B, which are distant events for IWi ('stationary observer') and local events for IOn ('moving observer'). Hence, (16) conforms to the spacetime interval invariance and no normalization factor is required. This confirms that all STGM axes in Fig. 1 represent time and space values to the same scale. (The end of Derivation 1)

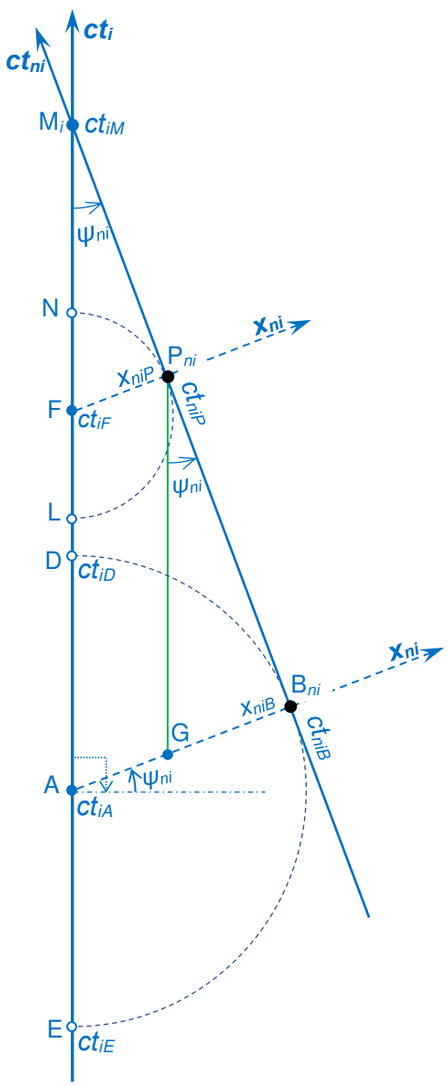


Figure 1. STGMi. IWi exists on main axis $\boldsymbol{ct_i}$. Radar signals are emitted at points E and L and detected at D and N. Semicircles $\overset{\frown}{ED^+}=O^+(A, r_{iB}=|AE|)$ and $\overset{\frown}{LN^+}=O^+(F, r_{iP}=|FL|)$ are the images of the distant reflection events B and P with reference points A and F; points B_{ni} and P_{ni} are the images of IOn at the instants ($\boldsymbol{ct_{iA}}$, $\boldsymbol{ct_{niB}}$) and ($\boldsymbol{ct_{iF}}$, $\boldsymbol{ct_{niP}}$) respectively; $\boldsymbol{ct_{ni}}$ and $\boldsymbol{x_{ni}}$ are time and movable space axes of IOn; M_i is the point of IWi–IOn collision. The drawing is valid for IWi.

Continuing to use $\measuredangle \mathrm{GB}_{ni}\mathrm{P}_{ni}$ and $\square\mathrm{AFP}_{ni}\mathrm{G}$, we may directly write the well-recognized ratio for the duration[1] between events B and P, $|\mathrm{B}_{ni}\mathrm{P}_{ni}|$ and $|\mathrm{AF}|$, independently measured by IOn and IWi. Below, the first relation is obtained from $\measuredangle \mathrm{GB}_{ni}\mathrm{P}_{ni}$. Then, we replace $|\mathrm{GP}_{ni}|$ with $|\mathrm{AF}|$ as the opposite side of $\square\mathrm{AFP}_{ni}\mathrm{G}$. Further, we isolate $\cos^2\psi_{ni}$ from the trig identity and take the square root to substitute $\cos\psi_{ni} = \sqrt{1-\sin^2\psi_{ni}}$. Finally, we arrive at velocity via (11)

$$|\mathrm{B}_{ni}\mathrm{P}_{ni}| = |\mathrm{GP}_{ni}|\cos\psi_{ni} = |\mathrm{AF}|\cos\psi_{ni} = |\mathrm{AF}|\sqrt{1-\sin^2\psi_{ni}} = |\mathrm{AF}|\sqrt{1-\frac{{V_{ni}}^2}{c^2}} \qquad (17)$$

We see the geometrical meaning of (17) from $\measuredangle \mathrm{GB}_{ni}\mathrm{P}_{ni}$ in Fig. 1: time leg $|\mathrm{B}_{ni}\mathrm{P}_{ni}|$ measured by the 'moving observer' IOn is always shorter than time hypotenuse $|\mathrm{GP}_{ni}|$ measured by 'stationary observer' IWi.

Now, we take into account the semicircles representing the interactions of IWi and IOn with the radar signals. Distinct from the initial scenario one may read from Fig. 1 that *a radio-signal* was *emitted* by IWi within time period $|\mathrm{EL}|$ and *received* by IOn within $|\mathrm{B}_{ni}\mathrm{P}_{ni}|$. Once this is noted, these time periods should conform to the relativistic Doppler effect. Let us check it.

Below we decompose $|\mathrm{EL}|$ using $|\mathrm{AF}|$ and combine the substitutions: $|\mathrm{AF}|=|\mathrm{GP}_{ni}|$ as the opposite sides of $\square\mathrm{AFP}_{ni}\mathrm{G}$, $|\mathrm{AE}|=|\mathrm{AB}_{ni}|$ as the radii of $O^+(\mathrm{A}, r_{iB}=|\mathrm{AE}|)$, and $|\mathrm{FL}|=|\mathrm{FP}_{ni}|=|\mathrm{AG}|$ as the radii of $O^+(\mathrm{F}, r_{iP}=|\mathrm{FL}|)$ and as the opposite sides of $\square\mathrm{AFP}_{ni}\mathrm{G}$. Then, we read from Fig. 1 $|\mathrm{AB}_{ni}|-|\mathrm{AG}|=|\mathrm{GB}_{ni}|$; and use $|\mathrm{GB}_{ni}|=|\mathrm{GP}_{ni}|\sin\psi_{ni}$ from $\measuredangle \mathrm{GB}_{ni}\mathrm{P}_{ni}$:

$$|\mathrm{EL}| = |\mathrm{AF}| + |\mathrm{AE}| - |\mathrm{FL}| = |\mathrm{GP}_{ni}| + |\mathrm{AB}_{ni}| - |\mathrm{AG}| = |\mathrm{GP}_{ni}| + |\mathrm{GB}_{ni}| = |\mathrm{GP}_{ni}| + |\mathrm{GP}_{ni}|\sin\psi_{ni} =$$

Proceeding further, we group the terms. Then, given $\measuredangle \mathrm{GB}_{ni}\mathrm{P}_{ni}$ we replace $|\mathrm{GP}_{ni}|$ with the ratio of $|\mathrm{B}_{ni}\mathrm{P}_{ni}|$ to $\cos\psi_{ni}$, substituting the latter with the root as in (17), and rearrange the expression

$$= |\mathrm{GP}_{ni}|(1+\sin\psi_{ni}) = |\mathrm{B}_{ni}\mathrm{P}_{ni}|\frac{1+\sin\psi_{ni}}{\sqrt{1-\sin^2\psi_{ni}}} = |\mathrm{B}_{ni}\mathrm{P}_{ni}|\sqrt{\frac{(1+\sin\psi_{ni})^2}{(1-\sin\psi_{ni})(1+\sin\psi_{ni})}} = |\mathrm{B}_{ni}\mathrm{P}_{ni}|\sqrt{\frac{1+\sin\psi_{ni}}{1-\sin\psi_{ni}}}$$

After the standard application of (11), we obtain Doppler's formula for time periods in 2D (Einstein gives the equation in reciprocal form,[1] for frequencies: $\nu=1/\mathrm{T}$)

$$|\mathrm{EL}| = |\mathrm{B}_{ni}\mathrm{P}_{ni}|\sqrt{\frac{1+\frac{V_{ni}}{c}}{1-\frac{V_{ni}}{c}}} \qquad (18)$$

One may also read from Fig. 1 that IOn *emits* a radio-signal within $|\mathrm{B}_{ni}\mathrm{P}_{ni}|$, and IW$i$ *receives* it within $|\mathrm{DN}|$. We then decompose $|\mathrm{DN}|$ using $|\mathrm{AF}|$ and, following the previous combined substitutions, we obtain $|\mathrm{DN}|=|\mathrm{GP}_{ni}|(1-\sin\psi_{ni})$. Further, as before, we express $|\mathrm{GP}_{ni}|$ in terms of $|\mathrm{B}_{ni}\mathrm{P}_{ni}|$, but now we isolate $|\mathrm{B}_{ni}\mathrm{P}_{ni}|$ (keeping $|\mathrm{DN}|$ on the right side) and naturally obtain the required equation relating $|\mathrm{B}_{ni}\mathrm{P}_{ni}|$ to $|\mathrm{DN}|$ in the same way as in (18).

Preceding examples demonstrate that the STGM faithfully represents the considered scenario, along with the spatio-temporal characteristics of the object and events. Moreover, since we applied no restrictions on IOn and IWi, the developed graphical scheme holds true for arbitrary pair of inertial agents. Hence, it may be used as a geometric core in further models. To this end, it is expedient to examine this drawing for extraction of specific construction procedures.

Considering $\boldsymbol{ct_{ni}}$ in Fig. 1, we see two options of the object's *time axis construction* (TAC) relative to main $\boldsymbol{ct_i}$.

TAC1. We can take one semicircle of *bonding event* (an observed event that involves the selected object, e.g. B or P) and touch it by the object's time axis $\boldsymbol{ct_{ni}}$, concurrently forming the tilt angle satisfying (8) and (11).

TAC2. We can position time axis $\boldsymbol{ct_{ni}}$ to be the tangent to both semicircles of bonding events B and P, as it was done in the beginning of Step 2.

The point of the agents' collision (e.g. M_i) can be also used in TAC1 and TAC2 as a degenerate semicircle (see Step 1).

Thus, any pair of these geometrical conditions, two bonding events and the tilt angle, is enough to construct the IO's time axis relative to the IW's one in compliance with the IO's velocity and with the IW's proper time.

If we additionally know the IO's instant at a bonding event, we label it on the IO's time axis at the point of tangency with the event's semicircle.

TAC1 and TAC2 enable one to add to STGM*i* time axes of any countable number of given objects.

When IO's time axis $\boldsymbol{ct_{ni}}$ is constructed as noted, it becomes *relevant* (close to referenced) to IW's time axis $\boldsymbol{ct_i}$ and we can complete the axes geometry with space axis $\boldsymbol{x_{ni}}$ (e.g. Fig. 1) by the following *space axis construction* (SAC) procedure.

SAC1. We aptly construct space axis $\boldsymbol{x_{ni}}$ perpendicular to $\boldsymbol{ct_{ni}}$ via (9).

SAC2 relative to $\boldsymbol{ct_i}$ via (10) and (11) is also possible.

The space axis intersects both time axes, uniquely connecting the instantaneous images of IW*i* and IO*n*, thereby interlinking the *spatio-temporal parameters* (STP) marked on all three axes: the object's coordinates (ct_i, x_{ni}) and proper time (ct_{ni}). Hence if we know any single value from the STP triplet (ct_i, x_{ni}, ct_{ni}), we may find the others via appropriate construction and translation of axis $\boldsymbol{x_{ni}}$. In particular we may read the STP at any instant shown by IW*i*'s or IO*n*'s clock.

For example, the STP of instantaneous object's image B_{ni} in Fig. 1, valid for IW*i*, we read as

$$B_{ni}(ct_{iB} = ct_{iA}, x_{niB} = |AB_{ni}|, ct_{niB}), \tag{19}$$

where the instants ct_{iA} and ct_{niB} can be provided by the respective segments containing origins, as soon as the latter are given on axes $\boldsymbol{ct_i}$ and $\boldsymbol{ct_{ni}}$. Say, the origins coincide at M_i; then we obtain: $ct_{iB}=-|M_iA|$ and $ct_{niB}=-|M_iB_{ni}|$.

Step 3. Graphical transformation of event's image and coordinates

The new problem conditions contain coordinates $x_{iB}\neq 0$, $ct_{iB}\neq 0$ of distant event B and the velocity of IW*j*, $V_{ji}\neq 0$, all measured by IW*i*. The task is to find the event coordinates x_{jB} and ct_{jB} valid for the new observer IW*j*, with the qualification that the proper time of IW*i* and IW*j* starts at the collision point, labeled Q.

The detailed solution to the problem is proposed in Appendix 1 in the Supplementary Information.

The resulting drawing is shown in Fig. 2. Blue and red time axes, $\boldsymbol{ct_i}$ and $\boldsymbol{ct_j}$, belong to IW*i* and IW*j* respectively. Blue semicircle $O^+(A, r_{iB}=|AW|)$ represents event B in STGM*i* according to given coordinates $ct_{iB}=|QA|$ and $x_{iB}=|AW|$. And red semicircle $O^-(H, r_{jB}=|HW|)$ corresponds to the target coordinates $ct_{jB}=|QH|$ and $x_{jB}=-|HW|$ valid in STGM*j*.

Light-blue axis $\boldsymbol{ct_{ni}}$ touching $O^+(A, r_{iB}=|AW|)$ and light-red $\boldsymbol{ct_{kj}}$ touching $O^-(H, r_{jB}=|HW|)$ represent two simulated objects, IO*n* and IO*k*, which are similar to 'stationary clocks'[1] located at event B and synchronized with the clocks of the outside observers IW*j* (IO*j*) and IW*i* (IO*i*) respectively. Complying with (11) and (8), the synchronized time axes of these agents are parallel: $\boldsymbol{ct_{ni}}\|\boldsymbol{ct_j}$ $(\boldsymbol{ct_{ji}})$ and $\boldsymbol{ct_{kj}}\|\boldsymbol{ct_i}$ $(\boldsymbol{ct_{ij}})$. In turn by (9), each of the axis pairs is perpendicular to the appropriate object's space axis, $\boldsymbol{x_{ni}}$ or $\boldsymbol{x_{kj}}$; further we will utilize: $\boldsymbol{x_{ni}}\perp\boldsymbol{ct_j}$ $(\boldsymbol{ct_{ji}})$ and $\boldsymbol{x_{kj}}\perp\boldsymbol{ct_i}$ $(\boldsymbol{ct_{ij}})$. Moreover, the space axes pass through black dot W (which covers blue and red superimposed images of IO*n* and IO*k* participating in event B: $B_{ni}\rightarrow W\leftarrow B_{kj}$). The geometric properties of these four axes detailed and justified in Appendix 1 enable us to make a step-by-step graphical *scheme for coordinates transformation* (SCT).

SCT. We substitute the relative velocity V_{ji} into (11) and obtain angle ψ_{ji}. Following (8), we form ψ_{ji} by blue $\boldsymbol{ct_i}(\boldsymbol{ct_{ij}})$ and red $\boldsymbol{ct_j}(\boldsymbol{ct_{ji}})$ in Fig. 2. Using their intersection Q as the origin, we mark given ct_{iB} by reference point A on blue $\boldsymbol{ct_i}$: $|QA|=|ct_{iB}|$ (upwards from Q for $ct_{iB}>0$, as in Fig. 2). From A we draw blue $\boldsymbol{x_{ni}}$ perpendicular to red $\boldsymbol{ct_j}$ and mark given x_{iB} on $\boldsymbol{x_{ni}}$ by black dot W: $|AW|=|x_{iB}|$ (to the right from A, for $x_{iB}>0$). Finally, from W we draw red axis $\boldsymbol{x_{kj}}$ perpendicular to blue $\boldsymbol{ct_i}$ until it intersects red $\boldsymbol{ct_j}$ at thus found point H, which is the reference point of event B in STGM*j*. Now, we read the *transformed coordinates*: $x_{jB}=-|HW|$ and $ct_{jB}=|QH|$ valid for IW*j* (we are to respect the signs of coordinates when mapping and reading).

In parallel, since universal point W and two reference points A and H determine the defining parameters of blue and red semicircles, we can develop a scheme for the *event image transformation* (EIT), without using coordinates.

EIT. To transform the image of event B from blue STGM*i* to red STGM*j* in Fig. 2, we orient the black-dashed radius of given blue O^+(A, r_{iB}=|AW|) perpendicular to red axis ct_j, thus obtaining the position of universal point W. From W we draw the black-dashed segment perpendicular to blue axis $\boldsymbol{ct_i}$ until it intersects red $\boldsymbol{ct_j}$ at reference point H, which provides the centre and radius of the desired red semicircle O^-(H, r_{jB}=|HW|).

The procedures inverse to SCT and EIT follow symmetrically.

Further, to confirm correctness of the obtained graphical schemes, we will derive Lorentz transformations from 4 similar right-angled triangles ⊿QMH, ⊿QNA, ⊿AMW and ⊿HNW ($\hat{Q} = \hat{W} = |\psi_{ji}|$) containing universal point W (see Fig. 2).

Derivation 2. Lorentz transformations.

We use right triangles ⊿HNW and ⊿QNA in Fig. 2 to express the space coordinate of event B, x_{jB}=x_{kjB}=−|HW|, in terms of x_{iB}=x_{niB}=|AW| and ct_{iB}=ct_{iA}=|QA|. Below, from ⊿HNW we substitute |HW|=|WN|/cosψ_{ij}. Then, we decompose |WN|=|AN|−|AW| and drag the minus to the difference in the numerator. Finally, using ⊿QNA and considering that sinψ_{ij}<0 (given ψ_{ij}<0) we replace '−|AN|' with |QA|sinψ_{ij}

$$x_{jB} = x_{kjB} = -|\mathrm{HW}| = -\frac{|\mathrm{WN}|}{\cos\psi_{ij}} = -\frac{|\mathrm{AN}|-|\mathrm{AW}|}{\cos\psi_{ij}} = \frac{-|\mathrm{AN}|+|\mathrm{AW}|}{\cos\psi_{ij}} = \frac{|\mathrm{QA}|\sin\psi_{ij}+|\mathrm{AW}|}{\cos\psi_{ij}}$$

With |QA|=ct_{iB} and |AW|=x_{iB}, we obtain

$$x_{jB} = \frac{ct_{iB}\sin\psi_{ij} + x_{iB}}{\cos\psi_{ij}} \qquad (20)$$

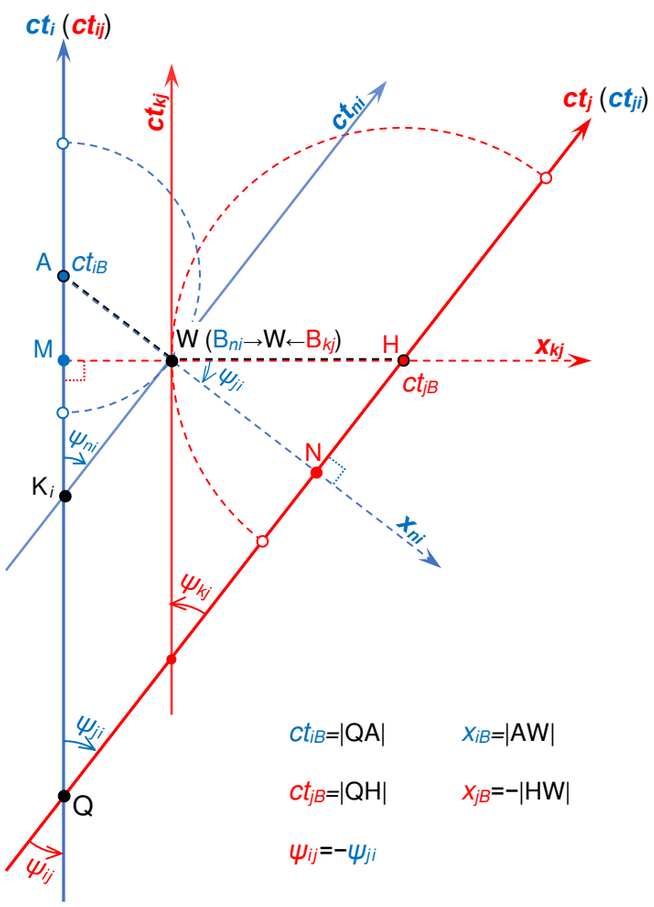


Figure 2. Graphical transformation of event coordinates, using universal point W. Blue STGM*i* is valid for observer IW*i* and red STGM*j* is valid for IW*j*. $\boldsymbol{ct_i}$ is the time axis of IW*i* in STGM*i*, but in STGM*j* we read it as $\boldsymbol{ct_{ij}}$ of IO*i*; $\boldsymbol{ct_j}$ is the time axis of IW*j* in STGM*j*, but in STGM*i* we read it as $\boldsymbol{ct_{ji}}$ of IO*j*; $\boldsymbol{ct_{ni}}$ and $\boldsymbol{x_{ni}}$ are time and space axes of IO*n* in STGM*i*, $\boldsymbol{ct_{kj}}$ and $\boldsymbol{x_{kj}}$ – of IOk in STGM*j*. Event B is represented in STGM*i* by blue semicircle O^+(A, r_{iB}=|AW|) and in STGM*j* – by red O^-(H, r_{jB}=|HW|). Black points Q and W are used in both models.

To transform the time coordinate $ct_{jB}=ct_{jH}=|\mathrm{QH}|$ we employ the right triangles ⊿QMH and ⊿AMW (see Fig. 2). Below, from ⊿QMH we express $|\mathrm{QH}|=|\mathrm{QM}|/\cos\psi_{ij}$. Then we decompose $|\mathrm{QM}|=|\mathrm{QA}|-|\mathrm{AM}|$. Further we substitute: $-|\mathrm{AM}|=|\mathrm{AW}|\sin\psi_{ij}$, considering ⊿AMW and respecting the sign of $\psi_{ij}<0$

$$ct_{jB}=ct_{jH}=|\mathrm{QH}|=\frac{|\mathrm{QM}|}{\cos\psi_{ij}}=\frac{|\mathrm{QA}|-|\mathrm{AM}|}{\cos\psi_{ij}}=\frac{|\mathrm{QA}|+|\mathrm{AW}|\sin\psi_{ij}}{\cos\psi_{ij}}$$

With $|\mathrm{QA}|=ct_{iB}$ and $|\mathrm{AW}|=x_{iB}$, we obtain

$$ct_{jB}=\frac{ct_{iB}+x_{iB}\sin\psi_{ij}}{\cos\psi_{ij}} \qquad (21)$$

Proceeding from ψ_{ij} to velocity in (20) and (21) by analogy with (17), we arrive at Lorentz's transformations:

$$x_{jB}=\frac{ct_{iB}\frac{V_{ij}}{c}+x_{iB}}{\sqrt{1-\frac{V_{ij}^{\ 2}}{c^2}}}, \qquad ct_{jB}=\frac{ct_{iB}+x_{iB}\frac{V_{ij}}{c}}{\sqrt{1-\frac{V_{ij}^{\ 2}}{c^2}}} \qquad (22)$$

Inverse transformations may be easily read from Fig. 2 in a similar way: one should consider right triangles ⊿AMW and ⊿QMH to express $x_{iB}=x_{niB}=|\mathrm{AW}|$ in terms of $x_{jB}=x_{kjB}=-|\mathrm{HW}|$ and $ct_{jB}=ct_{jH}=|\mathrm{QH}|$ (given $x_{iB}>0$, $\psi_{ji}>0$ and $x_{jB}<0$), and then, right triangles ⊿QNA and ⊿HNW to obtain the relation for $ct_{iB}=ct_{iA}=|\mathrm{QA}|$. The new relationships will be the same to (22) but swapped indexes *i* and *j*. The normal and inverse Lorentz's transformations obtain full symmetry when using the proposed set of subscripts, due to $V_{ji}=-V_{ij}$, as well as $\psi_{ji}=-\psi_{ij}$. (The end of Derivation 2.)

One may probably guess that Fig. 2 will resemble Loedel's symmetric STD[6] after deleting all semicircles and interpreting the space axes $\boldsymbol{x_{kj}}$ and $\boldsymbol{x_{ij}}$ as gridlines. However, as follows from the above, STGM is completely different from STD in physical meaning and construction (see Discussion also).

Step 4. Graphical transformation of object's time axis

Assume we have STGM*i* representing object IO*n* with velocity $V_{ni}\neq 0$, as in Fig. 1. STGM*i* consists of two blue axes $\boldsymbol{ct_i}$ and $\boldsymbol{ct_{ni}}$. Under (11) and (8) they form angle ψ_{ni} with vertex M_i implying IO*n*–IW*i* collision. We are also given velocity V_{ji}, $V_{ni}\neq V_{ji}\neq 0$, of new observer IW*j* and duration $|\mathrm{QM}_i|$, where Q is the point of IW*j*–IW*i* collision and their common origin of time. All data are valid for IW*i*.

The task is to draw STGM*j* for IW*j* in conformity with IW*j*'s velocity and proper time. In particular we are to transform the object's time axis: blue $\boldsymbol{ct_{ni}}$ valid for IW*i* into red $\boldsymbol{ct_{nj}}$ valid for IW*j*.

The solution begins with transferring the axes from Fig. 1 to Fig. 3. Here, given $|\mathrm{QM}_i|$, we mark point Q on blue axis $\boldsymbol{ct_i}$. From Q we draw red axis $\boldsymbol{ct_j}$, forming tilt angle ψ_{ji} related by (11) to IW*j*'s velocity V_{ji}. Thus, we apply techniques TAC1 in the way shown in SCT of Step 3.

Let us touch axis $\boldsymbol{ct_{ni}}$ in Fig. 3 by two blue semicircles centred at points A and F on axis $\boldsymbol{ct_i}$, $O^+(\mathrm{A}, r_{iB}=|\mathrm{AB}_{ni}|)$ and $O^+(\mathrm{F}, r_{iP}=|\mathrm{FP}_{ni}|)$. According to the substance of rule TAC2, these semicircles serve as the images of two distant bonding events B and P (simulated), and IO*n*'s participations are indicated by the tangent points B_{ni} and P_{ni}.

Now, applying EIT to these blue semicircles, we construct red semicircles $O^-(\mathrm{H}, r_{jW}=r_{jB}=|\mathrm{HW}|)$ and $O^-(\mathrm{G}, r_{jU}=r_{jP}=|\mathrm{GU}|)$ centred at reference points H and G (respectively obtained from A and F via universal points W and U). Reasoning from rule TAC2, we see that the tangent line to the red semicircles representing bonding events B and P in STGM*j* is the sought IO*n*'s time axis $\boldsymbol{ct_{nj}}$, valid for IW*j*. The task is completed.

The symmetry of Fig. 3 makes possible the inverse transformation: from red $\boldsymbol{ct_{nj}}$ to blue $\boldsymbol{ct_{ni}}$.

Moving forward, we find from Fig. 3 that time axes $\boldsymbol{ct_i}$, $\boldsymbol{ct_j}$, $\boldsymbol{ct_{ni}}$ and $\boldsymbol{ct_{nj}}$ are forming three angles analogous to (8):

$$\widehat{\overrightarrow{ct_i}\ \overrightarrow{ct_{ni}}}=\psi_{ni}\,, \qquad \widehat{\overrightarrow{ct_i}\ \overrightarrow{ct_j}}=\psi_{ji}\,, \qquad \widehat{\overrightarrow{ct_j}\ \overrightarrow{ct_{nj}}}=\psi_{nj} \qquad (23)$$

And since sines of these angles correlate by (11) to velocities V_{ni}, V_{ji} and V_{nj}, their composition seems to be of interest.

Preparing the drawing for further Derivation 3, we delete from Fig. 3 all semicircles and rename it as Fig. 4. Here we observe that the collision points N_j and M_i are analogous to K_i in Fig. 5 in Appendix1,

where we applied SAC at point K_i to reconstruct the reference point G of distant collision event K. Proceeding similarly in Fig. 4, we construct blue axis $\boldsymbol{x_{ji}}$ ($\boldsymbol{x_{ji}}\perp\boldsymbol{ct_{ji}}$) at point N_j ($\boldsymbol{x_{ji}}\cap\boldsymbol{ct_{ji}}=N_j$) and find reference point S ($S=\boldsymbol{x_{ji}}\cap\boldsymbol{ct_i}$), thus obtaining the centre and radius (r_{iN}) of blue semicircle $O^+(S, r_{iN}=|SN_j|)$, which is the image of distant (for IWi) collision event N in STGMi. IOj ($\boldsymbol{ct_{ji}}$) and IOn ($\boldsymbol{ct_{ni}}$) are involved in the event at tangent points N_j and N_{ni}. In turn, using M_i in STGMj, we analogously find reference point L and depict the distant (for IWj) event M as red semicircle $O^-(L, r_{jM}=|LM_i|)$ with radius r_{jM}. IOi ($\boldsymbol{ct_{ij}}$) and IOn ($\boldsymbol{ct_{nj}}$) are participating in this collision event at tangent points M_i and M_{nj}.

Derivation 3. Composition of velocities.

Let us express sines of the angles from (23) as ratios of sides of right triangles shown in Fig. 4. We obtain (24) for ψ_{ni} from $\measuredangle SN_{ni}M_i$, (25) and (26) for ψ_{ji} from $\measuredangle QN_jS$ and $\measuredangle QM_iL$, and the last (27) for ψ_{nj} from $\measuredangle LM_{nj}N_j$

$$\sin\psi_{ni} = -\frac{|SN_{ni}|}{|SM_i|} \qquad (24) \qquad\qquad \sin\psi_{ji} = \frac{|SN_j|}{|QS|} \qquad (25)$$

$$\sin\psi_{ji} = (-\sin\psi_{ij}) = \frac{|LM_i|}{|QL|} \qquad (26) \qquad\qquad \sin\psi_{nj} = -\frac{|LM_{nj}|}{|LN_j|} \qquad (27)$$

From (25) and (26) follows the proportion: $\dfrac{|SN_j|}{|QS|} = \dfrac{|LM_i|}{|QL|}$ (28)

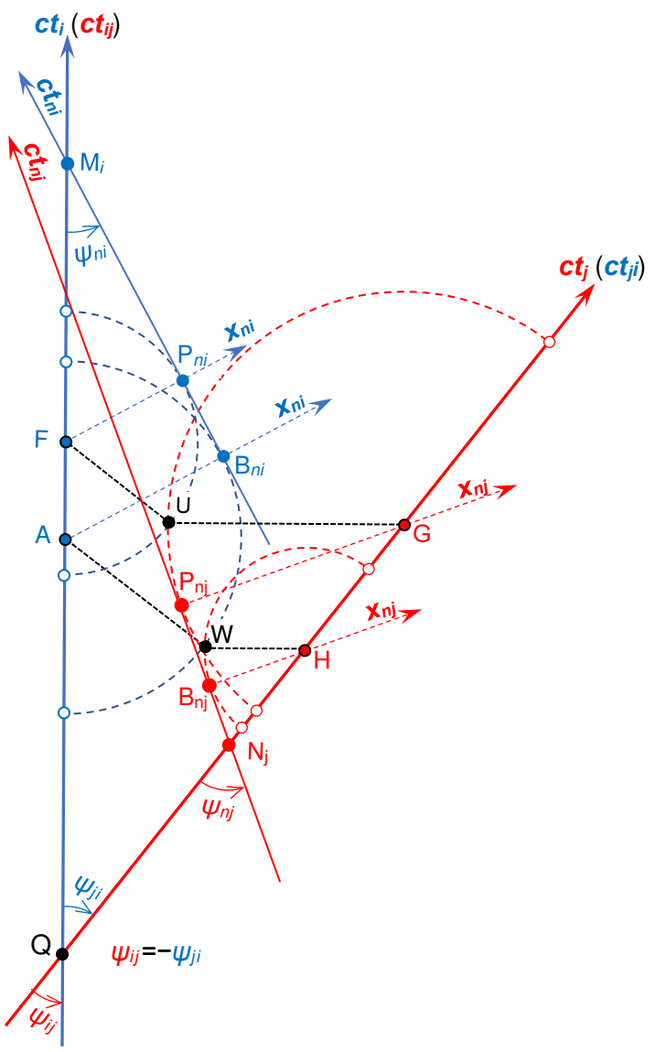


Figure 3. Transformation of IOn's time axis from blue STGMi (for IWi) to red STGMj (for IWj). $\boldsymbol{ct_i}$ is the main axis in STGMi, but it servs as $\boldsymbol{ct_{ij}}$ of IOi in STGMj; $\boldsymbol{ct_j}$ is the main axis in STGMj, but in STGMi it is $\boldsymbol{ct_{ji}}$ of IOj. Object IOn is represented by $\boldsymbol{ct_{ni}}$ and $\boldsymbol{x_{ni}}$ in STGMi, or by $\boldsymbol{ct_{nj}}$ and $\boldsymbol{x_{nj}}$ in STGMj. IOn participates in two distant events B and P, which are represented as blue semicircles $O^+(A, r_{iB}=|AW|)$ and $O^+(F, r_{iB}=|FU|)$ in STGMi or as red $O^-(H, r_{jB}=|HW|)$ and $O^-(G, r_{jB}=|GU|)$ in STGMj. Black points W and U are used for graphical transformations of the events' images. Black dotted lines are perpendicular to the opposite time axes ($\boldsymbol{ct_{ij}}$ or $\boldsymbol{ct_{ji}}$).

Below we intend to express the lengths in equation (24) in terms of those used in equations (25)–(27). First, we replace $|\mathrm{SN}_{ni}|$ with $|\mathrm{SN}_j|$ in the numerator, using that $|\mathrm{SN}_{ni}|=r_{iN}=|\mathrm{SN}_j|$, and decompose the length in the denominator as $|\mathrm{SM}_i|=|\mathrm{QM}_i|-|\mathrm{QS}|$. Then, we express $|\mathrm{SN}_j|$ in terms of proportion (28). And further, we drag minus to the difference in the denominator

$$\sin\psi_{ni} = -\frac{|\mathrm{SN}_{ni}|}{|\mathrm{SM}_i|} = -\frac{|\mathrm{SN}_j|}{|\mathrm{QM}_i|-|\mathrm{QS}|} = -\frac{|\mathrm{LM}_i||\mathrm{QS}|}{|\mathrm{QL}|(|\mathrm{QM}_i|-|\mathrm{QS}|)} = \frac{|\mathrm{LM}_i||\mathrm{QS}|}{|\mathrm{QL}|(|\mathrm{QS}|-|\mathrm{QM}_i|)} =$$

Proceeding, we express hypotenuse of $\measuredangle\mathrm{QN}_j\mathrm{S}$ as: $|\mathrm{QS}|=|\mathrm{QN}_j|/\cos\psi_{ji}$, decomposing on the move $|\mathrm{QN}_j|=|\mathrm{QL}|-|\mathrm{LN}_j|$, and in the denominator, we additionally substitute $|\mathrm{QM}_i|=|\mathrm{QL}|\cos\psi_{ji}$ using $\measuredangle\mathrm{QM}_i\mathrm{L}$. Next, we remove the brackets.

$$= \frac{|\mathrm{LM}_i|\frac{|\mathrm{QL}|-|\mathrm{LN}_j|}{\cos\psi_{ji}}}{|\mathrm{QL}|\left(\frac{|\mathrm{QL}|-|\mathrm{LN}_j|}{\cos\psi_{ji}}-|\mathrm{QL}|\cos\psi_{ji}\right)} = \frac{|\mathrm{LM}_i||\mathrm{QL}|-|\mathrm{LM}_i||\mathrm{LN}_j|}{|\mathrm{QL}|^2-|\mathrm{QL}||\mathrm{LN}_j|-|\mathrm{QL}|^2\cos^2\psi_{ji}} =$$

Thereafter, we take outside $|\mathrm{QL}|^2$ in the denominator and apply the trig identity as: $1-\cos^2\psi_{ji}=\sin^2\psi_{ji}$. Then, in the denominator we substitute $|\mathrm{LM}_i|=|\mathrm{QL}|\sin\psi_{ji}$ from $\measuredangle\mathrm{QM}_i\mathrm{L}$.

$$= \frac{|\mathrm{LM}_i||\mathrm{QL}|-|\mathrm{LM}_i||\mathrm{LN}_j|}{|\mathrm{QL}|^2\sin^2\psi_{ji}-|\mathrm{QL}||\mathrm{LN}_j|} = \frac{|\mathrm{LM}_i||\mathrm{QL}|-|\mathrm{LM}_i||\mathrm{LN}_j|}{|\mathrm{LM}_i|^2-|\mathrm{QL}||\mathrm{LN}_j|} =$$

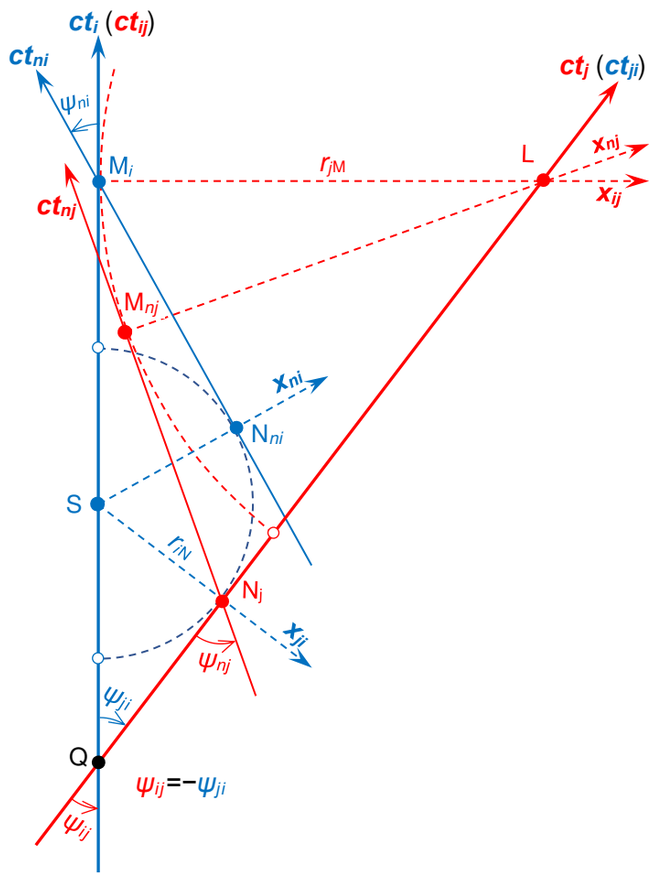


Figure 4. The representation of the scenario from Fig. 3 is adapted to derive Eq. (30). The baseline axes and notations correspond to those in Fig. 3. x_{ji} and x_{ij} are the space axes of IOi and IOj. Collision events N and M are represented as blue semicircle O^+(S, $r_{iN}=|\mathrm{SN}_j|$) and point M_i in STGMi, or as red point N_j and semicircle O^-(L, $r_{jM}=|\mathrm{LM}_i|$) in STGMj (the red semicircle is cropped).

Continuing, we divide the fractional expression by the product of lengths $|\mathrm{QL}||\mathrm{LN}_j|$. Now, replacing where necessary $|\mathrm{LM}_i|$ with $|\mathrm{LM}_{nj}|$ ($|\mathrm{LM}_i|=r_{jM}=|\mathrm{LM}_{nj}|$), we substitute the trig functions from (27) and (26), also respecting the signs $\psi_{nj}<0$ and $\psi_{ji}>0$.

$$= \frac{\frac{|\mathrm{LM}_{ji}|}{|\mathrm{LN}_j|} - \frac{|\mathrm{LM}_i|}{|\mathrm{QL}|}}{\frac{|\mathrm{LM}_i|^2}{|\mathrm{LN}_j||\mathrm{QL}|} - 1} = \frac{\frac{|\mathrm{LM}_{nj}|}{|\mathrm{LN}_j|} - \frac{|\mathrm{LM}_i|}{|\mathrm{QL}|}}{\frac{|\mathrm{LM}_{nj}||\mathrm{LM}_i|}{|\mathrm{LN}_j||\mathrm{QL}|} - 1} = \frac{-\sin\psi_{nj} - \sin\psi_{ji}}{-\sin\psi_{nj}\sin\psi_{ji} - 1}$$

Finally, we cancel "−1", rearrange the terms and obtain the following result:

$$\sin\psi_{ni} = \frac{\sin\psi_{ji} + \sin\psi_{nj}}{1 + \sin\psi_{ji}\sin\psi_{nj}} \tag{29}$$

Via (11) we arrive at velocities

$$V_{ni} = \frac{V_{ji} + V_{nj}}{1 + \frac{V_{ji}V_{nj}}{c^2}}, \tag{30}$$

where V_{ni} and V_{ji}, are the projections of IO*n*'s and IO*j*'s (IW*j*'s) velocities on axes $\boldsymbol{x_{ni}}$ and $\boldsymbol{x_{ji}}$, respectively, valid for (measured by) IW*i*; and V_{nj} is the projection of IO*n*'s velocity on axis $\boldsymbol{x_{nj}}$, valid for IW*j*. The sign of each substituting value depends on the relative direction of the velocity to the respective space axis. (The end of Derivation 3)

Equation (30) is the same as the well-known composition of velocities[1] (except designations). This proves the correctness of Step 4 and, with equations (16)–(18) and (22), the correctness of the proposed graphical approach, STGM, as a whole.

The graphical techniques obtained in Steps 1-4 are suitable for relativistic kinematic problems involving any countable number of inertial particle objects and observers, in the 2D case.

Applications of the method

The graphical solution to a kinematic problem starts with constructing STGM*i* by applying the techniques of Steps 1 and 2 to all available data valid for initial observer IW*i*: given velocities, object and event coordinates, and/or the proper time values measured by IW*i* and objects. When done, one obtains a single-scale STGM*i* containing time axes of the observer and objects as well as semicircles of events, all drawn in IW*i*'s specific colour (e.g. Fig. 1).

As shown in Step 2, one may immediately read from the constructed STGM*i* the following parameters:

- coordinates and proper time, STP (19), of any IO at any intersection of the IO's time and space axes constructed respectively via TAC and SAC procedures,
- durations measured independently by the IW and the IO (17), by appropriate translating of the IO's space axis (SAC),
- coordinates of any event (5), which are provided by the parameters of its semicircle (6) or obtained from the STP of an IO participating in the event, following the initial item above,
- the time periods of observer-object signal exchange with the Doppler effect taken into account (18), when using the semicircles,
- objects' velocities when applying (11) with (8) or (10).

The mentioned events and objects may also include simulated ones, as in Appendix 1 and Step 4.

As follows from the listed parameters, a single-observer drawing (STGM*i*) already contains useful information or even solution for particular tasks in particle physics and navigation (19), or communication (17) and (18).

Further, if required, one adds to the drawing the time axis $\boldsymbol{ct_j}$($\boldsymbol{ct_{ji}}$) of new observer IW*j*, applying TAC of Step 2 in the way shown in the SCT of Step 3. Then, via Steps 3 and 4, new STGM*j* is reconstructed from STGM*i* in the colour of IW*j*. The time axis of an outside observer serves as an object's axis with two indexes in each STGM. In addition to Steps 1–4, it is inherently possible to apply any available geometrical or trigonometric means, as in Derivations 1-3, for example.

The final drawing is composed of different-coloured STGM*i* and STGM*j* (analogous to Fig. 3 or 4, $V_{ji} \neq 0$). It represents to the same scale the above-listed parameters of objects and events, valid for each observer individually. The problem solution can be read from the models in any required format, as numerical data, e.g. (19), or as relationships, e.g. (16)–(18), (22) and (30).

Notably, the described steps of data mapping and reading predominantly employ geometric constructions, except for equations (8), (10) and (11), which require angular measures and trigonometric calculations. But we can substantially streamline the STGM usage by embedding the definition of velocity 'distance per unit time'.

Suppose, given an IO*i*'s velocity V_{ni}, we need to orient IO*i*'s axis $\boldsymbol{ct_{ni}}$ relative to main axis $\boldsymbol{ct_i}$ in blue STGM*i* (see Fig. 2, free from the earlier-used scenario). We then mark segment $|K_iA|=c$ d.u. (dropping units) on $\boldsymbol{ct_i}$, construct semicircle $O^{\pm}(A, r_{ni}=|V_{ni}|)$, using the sign (±) and value of V_{ni} ($V_{ni}>0$ in Fig. 2), and draw $\boldsymbol{ct_{ni}}$ through K_i as the tangent. Thus, we obtain the inter-axis angle ψ_{ni} without calculations. (Now, to finish TAC1 we aptly translate $\boldsymbol{ct_{ni}}$ to touch the semicircle of a given bonding event; not shown in Fig. 2)

And inversely, if we need to read IO*i*'s velocity V_{ni} from an existing drawing (Fig. 2, as previously), we mark off time period $|K_iA|=c$ d.u. on $\boldsymbol{ct_i}$ from collision point K_i and draw axis $\boldsymbol{x_{ni}}$ at point A perpendicular to $\boldsymbol{ct_{ni}}$ (SAC1). The latter axes intersection B_{ni}(W) marks on $\boldsymbol{x_{ni}}$ value $x_{niB}=V_{ni}=\text{sgn}(x_{niB})|AB_{ni}|$ d.u. Thus, we obtain the velocity as the segment length.

Summarizing, the described approach enables us to represent a relativistic kinematic scenario as a single-scale STGM for one IW, then to construct the new STGM for the other IW, complying with a given relative velocity and maintaining the same scale, and finally to read the problem solution from both STGM, all by *purely graphical techniques*.

Discussion

It seems useful to compare the developed STGM with Minkovsky-Loedel's symmetric STD[2,6] to ascertain the novelty of the proposed graphical approach. Both graphical methods employ the same formula (11) relating the inter-axis angle to the relative velocity. But the meaning, purposes and constructions of the methods are rather different.

A symmetric STD[6] typically comprises two coordinate systems having the same scale by virtue of this formula. So formed coordinate plains may be simultaneously applied to the *universal* (valid for two observers) picture of the *whole world spacetime*, enabling one to read both sets of coordinates of *any world-point*,[2] e.g. P (x, t, x', t') in Fig. 1.[8] We may also note, coming closer to the STGM, that one can compare the intervals marked on the observers' same-scale time axes. But this does not hold for a *worldline*[2] tracing an object with different velocity, since its time scale requires dual calibration.

Regarding the STGM, in terms of Minkowski,[2] it aims exclusively to represent 'substantial points': the images of objects and observers existing on their *time axes* (TAC), which in turn are analogous to worldlines in this context. But by contrast to a STD, all timelines (time axes) in the STGM, including objects' ones, maintain identical scales when carrying proper time data of their owners (related to a respective observer).

The space axis application in the STGM is also unusual. The movable *space axis* (SAC) connects an instantaneous image of the main IW with the simultaneous image of the observed IO when intersecting their relevant time axes (TAC). Only these two points are meaningful on the STGM space axis. And it primary serves to locate the agents' position when reading the object's STP (19) or constructing a semicircle (as shown in Steps 3 and 4).

Given the above, any empty world-point is useless in a STGM. Foreseeing this, in Step 1 we considered a reflection event (a world-point, marked by a substantial point). We represented it as a semicircle (6) and termed a 'graphical image of distant event'. Such a *semicircle* displays in the STGM the current position of a radar signal emitted by the considered IW (say, at point E in Fig. 1). The radius of the semicircle increases as its centre (reference point A) moves ($r=|EA|$). Any tangent of the semicircle with an IO's relevant time axis indicates that a bonding event of reflection (B) just happens. And the reflected signal will return to the IW (at D, the point of closure) after the symmetric period of time ($|AD|=|EA|$). So, the semicircle represents no less than two substances: the radar signal and at list one object, when considering its physical significance.

To conclude, the STGM does not qualify as a STD or as a part of it, due to the absence of any coordinate plane: we are not able to read coordinates of a separate (empty) point, if it (expectedly) does not belong to a constructed time axis and/or semicircle. Thus, since the STGM provides the spatio-temporal

characteristics of objects (17)–(19), and events (5), (6) by these geometric shapes, it should be termed a drawing or a graphical model, as previously proposed.

Unlike a STD displaying a universal picture of the world, the STGM represents a concrete *kinematic scenario*, for a concrete (single) inertial observer. But with this individualization we obtain universal (valid for all object-observer pairs) *geometric rules* (Steps 1–4) for relativistic data mapping, processing and reading, all *to the same scale*.

The STGM construction is based on the proper time physical measurements carried out by assigned observer and on the constancy of light speed as well. It does not rely on any reference frames and SR equations which are commonly used in the development of most established graphical techniques (e.g. [2,3,4,6,8]...).

Conclusion

The aim of this paper was to reveal the core idea of the STGM method and to illustrate its accuracy with some simple examples put into 2D conceptual spacetime within inertial and particle assumptions.

It was shown that this graphical approach can provide an efficient calculation-free solution, advantageously supplementing coordinates with proper time (19) for each object. Correctness of the obtaining data was approved by reading the main SR relationships (see Derivations 1–3) and well-known equations, (16)–(18) and (22), from the ready-made drawings. Moreover, the approach herein has no extra restrictions since it is based on pure geometry and no axiomatic statements have been added to the SR framework. Thus, the applicability of the STGM method for the graphical solving of kinematic problems within the scope similar to that of SR theory appears to be justified. The STGM method may be useful in particle physics, cosmology and related fields (see Applications).

There are no technical difficulties to add one more space dimension to the model and thus to expand the range of tasks. The development of three-dimensional STGM including its application for relativistic Doppler effect is almost complete.

Conceivably, a closer conceptual analysis of this approach would yield a fresh interpretation of space-time relationships via the principles and terms of geometry.

Data availability

All data generated or analyzed in this study are included in this article and in the Supplementary Information.

References

1. Einstein, A. On the Electrodynamics of Moving Bodies. In *The Principle of Relativity* (trans. Perrett, W. & Jeffery, G.B.) 35–65 (Methuen and Company, Ltd., 1923).
2. Minkowski, H. Space and Time. In *Minkowski's Papers on Relativity* (trans. Lewertoff, F. & Petkov, V., ed. Petkov, V.) (Minkowski Institute Press, 2012; see minkowskiinstitute.org/mip/).
3. Benedetto, E., Capriolo, M., Feoli, A. & Tucci, D. The twin paradox in a Loedel diagram. *Eur. J. Phys.* **39**, 045707 (2018). **doi:10.1088/1361-6404/aab335**
4. Maritz, M. F. & Hoffman, M. J. A three-dimensional interpretation of Minkowski spacetime. *Eur. J. Phys.* **47**, 025606 (2026). **doi:10.1088/1361-6404/ae46fa**
5. Bondi, H. *Relativity and Common Sense*. (Dover Publications, 1980).
6. Loedel, E. Aberración y Relatividad. *An. Soc. Cient. Argent.* **145**, 3–13 (1948).
7. Poincaré, H. Sur la dynamique de l'électron. *Rend. Circ. Mat. Palermo* **21**, 129–176 (1906). **doi:10.1007/BF03013466**
8. Gruner, P. & Sauter, J. Représentation géométrique élémentaire des formules de la théorie de la relativité. *Arch. Sci. Phys. Nat.* **3**, 295–296 (1921).

Supplementary Information

Appendix 1. Graphical transformation of event coordinates (detailed solution to Step 3, based on Steps 1 and 2)

We need to transform event B's coordinates $x_{iB}\neq 0$ and $ct_{iB}\neq 0$ valid for IWi into coordinates x_{jB} and ct_{jB} valid for IWj; given relative velocity $V_{ji}\neq 0$ and with the qualification that the observers' proper time measurements start at the collision point named Q.

Initially, we draw in Fig. 5 blue axis $\boldsymbol{ct_i}$ of IWi and mark points Q and A, $|QA|=ct_{iB}$. Proceeding from (5) and (6), we construct the image of event B as blue semicircle $O^+(A, r_{iB}=|x_{iB}|)$ centred at reference point A (Fig. 5 satisfies $x_{iB}>0$).

Now we intend to position the time axis of IWj, but the techniques of Step 2 were established only for IO's axis. Hence, we interpret IWj as IOj and, via TAC1, construct the agent's axis $\boldsymbol{ct_{ji}}$ in STGMi: we substitute velocity V_{ji} into (11) and orient $\boldsymbol{ct_{ji}}$ at obtained angle ψ_{ji} to main $\boldsymbol{ct_i}$ concurrently intersecting the latter at point Q given as the (local) bonding event of collision. Thus, we obtain $\boldsymbol{ct_{ji}}$ relevant to $\boldsymbol{ct_i}$ in STGMi, but we colour $\boldsymbol{ct_{ji}}$ in red.

Let us simulate agent IOn, who shares IOj's velocity, $V_{ni}=V_{ji}$, and participates in event B. To construct IOn's axis $\boldsymbol{ct_{ni}}$ in STGMi, we again apply TAC1. Due to equal velocities of the agents, new angle ψ_{ni} obtained from (11) repeats ψ_{ji}, $\psi_{ni}=\psi_{ji}$, meaning that blue $\boldsymbol{ct_{ni}}$ is parallel to red $\boldsymbol{ct_{ji}}$, $\boldsymbol{ct_{ni}}\|\boldsymbol{ct_{ji}}$ (8). And since IOn participates in bonding event B, blue $\boldsymbol{ct_{ni}}$ touches blue $O^+(A, r_{iB}=|x_{iB}|)$, at point B_{ni}, as shown in Fig. 5. So constructed $\boldsymbol{ct_{ni}}$ is relevant to main $\boldsymbol{ct_i}$. Later we will use the axes' intersection K_i, which represents local (for IWi) collision event K in STGMi, marking on each of the axes the image and the instant of the respective colliding agent.

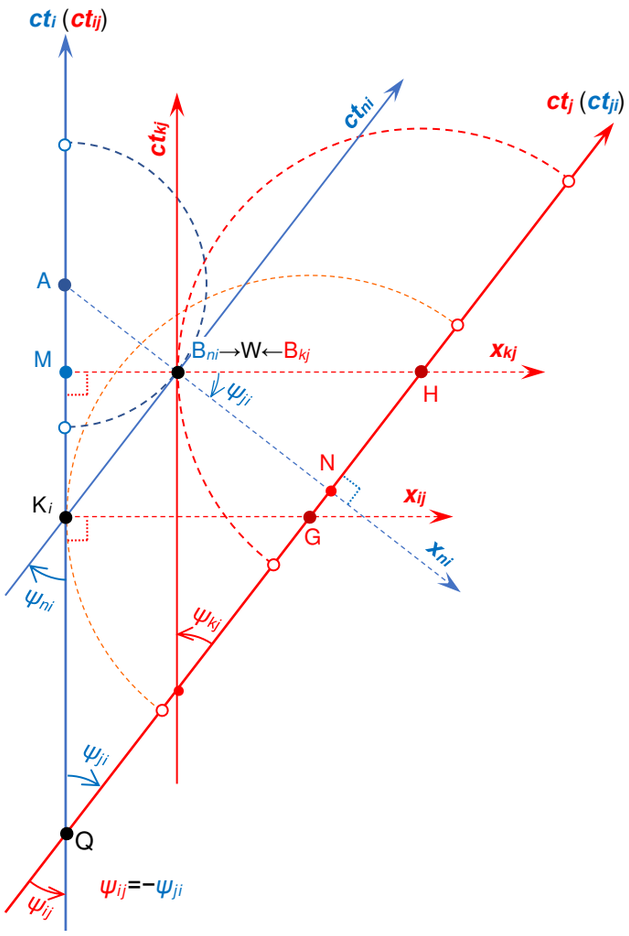


Figure 5. Graphical transformation of event B coordinates from blue STGMi to red STGMj, using auxiliary event K and simulated objects IOn and IOk. IWi's axis $\boldsymbol{ct_i}$ is the main axis in STGMi, but in STGMj it is renamed as $\boldsymbol{ct_{ij}}$ of IOi associated with $\boldsymbol{x_{ij}}$ as well; IWj's axis $\boldsymbol{ct_j}$ is the main in STGMj, but in STGMi it is $\boldsymbol{ct_{ji}}$ of IOj. IOn is represented by axes $\boldsymbol{ct_{ni}}$, $\boldsymbol{x_{ni}}$ in STGMi and by $\boldsymbol{ct_{nj}}$, $\boldsymbol{x_{nj}}$ in STGMj. Blue semicircle $O^+(A, r_{iB}=|AE|)$ corresponds to event B in STGMi; red $O^-(G, r_{jK}=|GK_i|)$ and $O^-(H, r_{jB}=|HB_{ni}|)$ respectively represent events K and B in STGMj. Black points Q, K_i and W are used in both STGM.

Now, intending to switch to red STGMj, we interchange the object-observer interpretation, from IWi–IOj to IOi–IWj, and rename their time axes: blue $\boldsymbol{ct_i}$ as object's $\boldsymbol{ct_{ij}}$ and red $\boldsymbol{ct_{ji}}$ as main $\boldsymbol{ct_j}$. This operation reverses the readout of ψ_{ij} since it is referenced to new main axis $\boldsymbol{ct_j}$ in STGMj, yielding: $\psi_{ij}=-\psi_{ji}$. But in spite of the opposite sign, ψ_{ij} again satisfies (8) and (11) because the velocity sign is also reversed, $V_{ij}=-V_{ji}$, due to switching the observation direction. Further, point Q still serves as the common origin of time and indicates the agents' collision applicable as a bonding event. Thereby fulfilled conditions of TAC1 mean that axis $\boldsymbol{ct_{ij}}$ is relevant to $\boldsymbol{ct_j}$ in STGMj.

Notably, the symmetry of the axis relevance ($\boldsymbol{ct_i}$–$\boldsymbol{ct_{ji}}$ and $\boldsymbol{ct_{ij}}$–$\boldsymbol{ct_j}$) shows that the applied TAC also allows to construct the double-designated axis of an outside observer, e.g. $\boldsymbol{ct_j}(\boldsymbol{ct_{ji}})$ or $\boldsymbol{ct_i}(\boldsymbol{ct_{ij}})$.

As previously verified by (16), two relevant time axes share the same scale in STGM. Hence, the performed renaming of the axes does not alter the lengths of marked instants. Thus, in STGMj, point K_i retains its position and continues to indicate (on $\boldsymbol{ct_{ij}}$) the instant shown by the clock of agent i (now named IOi) at participation in collision event K.

But as applied to IWj, this collision K is a distant event, which, according to Steps 1 and 2, should be represented in STGMj as the appropriate semicircle centred at the reference point corresponding to IWj's image at the event moment. Since $\boldsymbol{ct_{ij}}$ is relevant to $\boldsymbol{ct_j}$, we can legitimately use SAC1 to reconstruct the target image of IWj from existing image of IOi (K_i) by axis $\boldsymbol{x_{ij}}$. In Fig. 5 we erect $\boldsymbol{x_{ij}}$ at point K_i, $\boldsymbol{x_{ij}}\perp\boldsymbol{ct_{ij}}$, and it intersects main red $\boldsymbol{ct_j}$ marking the sought reference point G (K_i and G in red STGMj are analogous to B_{ni} and A in blue STGMi). With centre G we successively obtain radius $r_{jK}=|GK_i|$, and draw $O^-(G, r_{jK}=|GK_i|)$ in light-red colour. (The event K coordinates are: $ct_{jK}=|QG|$ and $x_{jK}=-|GK_i|$, if needed.)

Optionally, the position of IOn's time axis in STGMj ($\boldsymbol{ct_{nj}}$) can be determined by TAC1. When switching from STGMi to STGMj, equality $V_{ni}=V_{ji}$ turns into $V_{nj}=0$. By (11) and (8), this yields $\psi_{nj}=0$ and implies $\boldsymbol{ct_{nj}}\|\boldsymbol{ct_j}$. Concurrently, $\boldsymbol{ct_{nj}}$ touches light-red semicircle $O^-(G, r_{jK})$, at point K_{nj} (as shown in Fig. 6), due to said IOn's participation in event K. One could continue this reasoning, using axes $\boldsymbol{ct_{ni}}$, $\boldsymbol{ct_{nj}}$ and rectangle $\square GK_{nj}B_{nj}H$ to observe that $|K_iB_{ni}|=|K_{nj}B_{nj}|=|GH|$ and thus to find the event B's reference point H, which provides the required coordinates in STGMj. However, a shorter path is possible.

We are going to carry time interval $|K_iB_{ni}|$ from blue axis $\boldsymbol{ct_{ni}}$ to red axis $\boldsymbol{ct_j}$ right in Fig. 5. But we cannot do this immediately. Blue axis $\boldsymbol{ct_{ni}}$ is relevant only to main axis $\boldsymbol{ct_i}$ in blue STGMi, and it does not exist in red STGMj (any bonding event for $\boldsymbol{ct_{ni}}$ and $\boldsymbol{ct_j}$ axes is not available until the observers have nonzero relative velocity). Since $\boldsymbol{ct_{ni}}$ and $\boldsymbol{ct_j}$ are not relevant, Step 2 is inapplicable and we need to find another pattern in the STGM drawing.

On one hand, Fig. 5 shows $|K_iB_{ni}|$ as the duration between consecutive events K and B, which was measured by IOn's clock. And substituting $V_{nj}=0$ in (17) demonstrates that IWj's (IOj's) clock will measure equal time interval.

On the other hand, as mentioned, two relevant axes share the same scale (16). Sequentially applying this corollary to same-coloured time axes $\boldsymbol{ct_{ni}}$–$\boldsymbol{ct_i}$ and further to the different-coloured $\boldsymbol{ct_i}$–$\boldsymbol{ct_{ij}}$ and $\boldsymbol{ct_{ij}}$–$\boldsymbol{ct_j}$, as shown to be relevant, we observe that all these axes in the STGM drawing have the same scale. (This can be expanded on all axes in any STGM drawing.) In particular we obtain that two equal time intervals marked on the axes $\boldsymbol{ct_{ni}}$ and $\boldsymbol{ct_j}$ will have identical lengths.

Based on these arguments, we extend the length $|K_iB_{ni}|$ on red $\boldsymbol{ct_j}$ forward from reference point G (from the time mark of event K in STGMj). For this we draw the line segment $B_{ni}H$ parallel to K_iG (see Fig. 5), and, taking into account earlier mentioned parallelism of the time axes $\boldsymbol{ct_{ni}}\|\boldsymbol{ct_{ji}}$ ($\boldsymbol{ct_j}$), we obtain parallelogram $\square K_iB_{ni}HG$ ensuring the desired $|K_iB_{ni}|=|GH|$. We interpret so found point H as the reference point of event B since it marks (on axis $\boldsymbol{ct_j}$) the proper time of IWj at the event moment. Thus, via (3), the *time coordinate* of event B in STGMj is: $|QH|=ct_{jH}=ct_{jB}$.

Fig. 5 provides the required space coordinate as well. The mentioned zero velocity of IOn in STGMj, $V_{nj}=0$, means that the radar distance to him remains unchanged: $r_{jB}=r_{jK}=|GK_i|$. In turn, $|GK_i|=|HB_{ni}|$ as seen from $\square K_iB_{ni}HG$. So, we read the *space coordinate* of event B in STGMj as $x_{jB}=-r_{jB}=-|HB_{ni}|$. The task is completed.

Let us draw red semicircle $O^-(H, r_{jB})$ of event B, and take a closer look at Fig. 5. We observe that red $O^-(H, r_{jB})$ runs over blue $O^+(A, r_{iB})$ at the graphical dot B_{ni} (due to $r_{jB}=|HB_{ni}|$ and $r_{iB}=|AB_{ni}|$). But these

semicircles do not have any intersection since they belong to different STGM. To use a simile, each STGM looks like a single-colour tree, drawn on a separate transparent film. Then the 'trees' are overlaid, so that the axes of the observers coincide ($\boldsymbol{ct_i}$ is aligned with $\boldsymbol{ct_{ij}}$ and $\boldsymbol{ct_j}$ is aligned with $\boldsymbol{ct_{ji}}$), and pinned at single intersection Q. Hence, 'overlay' and 'superposition' are preferred terms. (This holds for single-colour semicircles too: since each semicircle contains the points with a unique set of coordinates, the semicircles' intersection possessing two different sets is meaningless. The only type of intersection for a semicircle is the tangent point with a relevant time axis when representing bonding event, as noted in Step 2.)

Thus, we obtain that point B_{ni} is overlapped by a point of the red semicircle. If singled out, this point (labeled B_{kj} in STGMj) brings into consideration the new object (IOk) participating in event B. Aiming to determine IOk's velocity V_{kj}, we connect B_{kj} with reference point H by space axis $\boldsymbol{x_{kj}}$ in Fig. 5. And we observe that $\boldsymbol{x_{kj}}$ is parallel to $\boldsymbol{x_{ij}}$ ($\boldsymbol{x_{kj}}\|\boldsymbol{x_{ij}}$) since these axes are containing the opposite sides ($|HB_{kj}|$ and $|GK_i|$) of parallelogram $\square K_iB_{kj}HG$. Sequentially applying (10) and (11) yields $\psi_{kj}=\psi_{ij}$ and shows that IOk shares the same velocity with IOi (IWi): $V_{kj}=V_{ij}$.

Given the mentioned properties of the simulated objects, IOn and IOk, we can interpret them as 'stationary clocks'[1] positioned at the location of event B and synchronized with the personal clocks of IWj and IWi respectively. IOn is represented in STGMi by $\boldsymbol{ct_{ni}}$ containing B_{ni}, and IOk is represented in STGMj by $\boldsymbol{ct_{kj}}$ containing B_{kj}.

We see from Fig. 5 that the superimposed points B_{ni} and B_{kj} anchor the reference points A and H, thus establishing the graphical relationship (bridge) between the STGMi's and STGMj's sets of the event coordinates. For the sake of convenience, we cover B_{ni} and B_{kj} with black dot W ($B_{ni}\rightarrow W\leftarrow B_{kj}$) having no physical meaning but valid for usage in both STGM, i and j.

The described geometric properties of the models are used in Step 3 to propose a simple step-by-step scheme for the graphical transformation of coordinates.

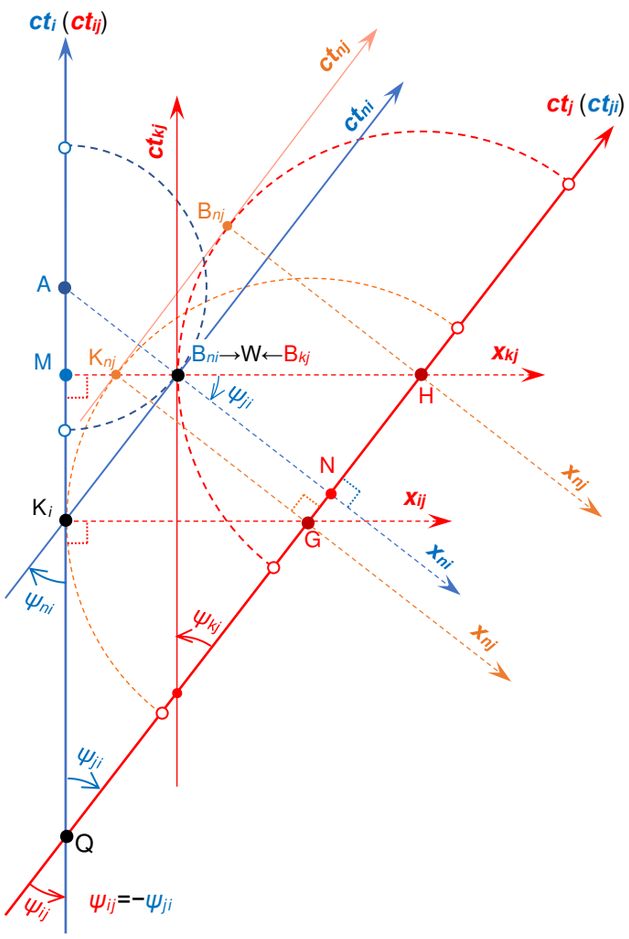


Figure 6. Graphical transformation of event B coordinates from blue STGMi (for IWi) to red STGMj (for IWj) with additional axes $\boldsymbol{ct_{kj}}$ and $\boldsymbol{x_{kj}}$ representing IOk in STGMj. The baseline axes and notations correspond to those in Fig. 5.